COMPARISON OF MONOENERGETIC PHOTON ORGAN DOSE RATE COEFFICIENTS FOR THE FEMALE STYLIZED AND VOXEL PHANTOMS SUBMERGED IN AIR

M. M. Hiller[1] and S. A. Dewji[1,*]
[1]Oak Ridge National Laboratory, Center for Radiation Protection Knowledge, P.O. Box 2008 MS 6335, Oak Ridge, TN 37831-6335

Received month date year, amended month date year, accepted month date year

Abstract Dose rate coefficients computed using the International Commission on Radiological Protection (ICRP) reference adult female voxel phantom were compared with values computed using the Oak Ridge National Laboratory (ORNL) adult female stylized phantom in an air submersion exposure geometry. This is a continuation of previous work comparing monoenergetic organ doses rate coefficients for the male adult phantoms. With both the male and female data computed, effective dose rate as defined by ICRP Publication 103 was compared for both phantoms. Organ dose rate coefficients for the female phantom and ratios of organ dose rates for the voxel and stylized phantoms are provided in the energy range from 30 keV to 5 MeV. Analysis of the contribution of the organs to effective dose is also provided. Comparison of effective dose rates between the voxel and stylized phantoms was within 8% at 100 keV and is < 5% between 200 and 5000 keV.

INTRODUCTION

The Center for Radiation Protection Knowledge (CRPK) at Oak Ridge National Laboratory (ORNL) is conducting a comprehensive effort to calculate gender and age-specific dose rate coefficients for external exposure of stylized phantoms to photons and electrons emitted by radionuclides distributed in air, water and soil[1, 2]. This paper builds upon previous work by Bellamy et al.[2] that compared organ doses of the International Commission on Radiological Protection (ICRP) Publication 110 adult male voxel phantom[3] to the updated ORNL stylized phantom by Han et al. [4] for a male phantom fully submerged in air. In the scope of the initial work, Bellamy et al. reported comparisons of organ dose rate coefficients for both the male stylized and voxel phantoms for monoenergetic photon energies ranging from 30 keV to 5000 keV. [2]

The use of an infinite air medium calculation has been derived from the traditional practice of dividing the infinite medium by a factor of two, accounting for the air–ground interface dose for submersion in an infinite medium[2] [5] [6] [7] [8].

In addition to the work by Bellamy et al. on the male phantom comparison, previous work by Kramer et al.[9] identified a difference of ~10% in effective dose between the phantom models for photon energies greater than 500 keV, and a difference of 10–20% for photon energies between 100 and 500 keV.

The work described here reports the organ dose rate coefficients of the ICRP Publication 110 female voxel phantom[3] and compares these to the ORNL female stylized phantom[4]. With the computation of both male (from Bellamy et al.[2]) and female organ dose rate coefficients derived here, effective dose rates, as described by ICRP Publication 103[10], using the voxel and the stylized phantoms of each gender were computed and compared.

*Corresponding author: dewjisa@ornl.gov

Furthermore, with the availability of male and female organ dose rate coefficients, any deviation in comparing the effective doses are identified and discussed in both the male and female voxel and stylized phantoms.

METHODOLOGY

Calculations presented here reflect the methods employed by calculations with the male phantoms by Bellamy et al.[2], but paralleled with the ICRP Publication 110 adult female voxel phantom[3] and ORNL adult female stylized phantom[4]. The ICRP adult female voxel phantom consists of 14.255124×10^6 voxels of which 3.88602×10^6 are the tissues of the phantom, the other voxels are describing the surrounding of the phantom; they are filled with air in the case discussed here. The phantom is oriented along a Cartesian coordinate system with the *x*-axis from the left to the right of the phantom, the *y*-axis from the front to the back of the phantom and the z-axis from the bottom to the top of the phantom; there are 299 voxels in the *x*-direction, 147 voxels in the *y*-direction, and 346 voxels in the *z*-direction. Each voxel has in-plane resolution of 1.775 mm, with a total of 53 distinct material compositions defining the phantom[3].

The adult female stylized phantom was originally developed at ORNL by Cristy and Eckerman in 1987[11] and modified two decades later by Han et al.[4]. The modified ORNL adult female stylized phantom[11] included revisions to organ elemental compositions to better reflect ICRP Publication 103 organs and tissues[10]. This included modifications to the head, brain, salivary glands, respiratory tract, extra-pulmonary airways, alimentary tract, rectosigmoid colon, urinary bladder mucosa wall, and kidneys. In addition to the modifications by Han et al.[4], minor revisions were made to radiation transport parameters in the stylized phantoms[1, 2, 11], including updates to the assigned organ volumes. The ORNL stylized phantom contains all organs included in the effective dose, as specified in ICRP Publication 103[10] with the exception of the extrathoracic region and the lymphatic system, for which the thymus serves as surrogate. The female stylized phantom consists of ~100 mathematical volumes representing body tissues and organs, and comprises 23 distinct material compositions defining the phantom. While the female voxel phantom employed here is based on the phantom in ICRP Publication 110[3], minor modifications were made in the material composition, density, organ/tissue volume and geometry. In the scope of this work, in accordance with the work by Bellamy et al.[2], tissue masses, compositions and densities were updated in to comply with ICRP Publication 89[12] and ICRU Report 46[13].

The computation of female photon organ dose rate coefficients using the voxel and stylized phantoms were conducted by use of the Monte Carlo N-Particle Transport Code ver. 6.1.1 (MCNP 6.1.1). [14] Paralleling the methodology employed with the male[2], calculations of dose rate coefficients considered the female voxel and stylized phantoms submersed in the center of an infinite cloud of contaminated air. The elemental composition and 1.2 kg m^{-3} density of air, 40% relative humidity, and 760 mmHg pressure mimic that of the male case (Table 1 of Ref [2]). The contaminated air environment was modeled in MCNP 6.1.1 as a rectangular parallelepiped with dimensions 1.1 × 0.8 × 2.85 m. The contaminated air environment employed the reflective boundary condition function in MCNP 6.1.1 such that the photon incident on the boundary fully reflects with no associated energy loss, hence representing an infinite cloud.

Radiation transport simulations in MCNP 6.1.1 were conducted in two phases. First, the collided and uncollided (scattered and unscattered) photon angular and energy-dependent fluences due to contaminated air were calculated by using a coupling surface surrounding the phantom location without the phantom embedded. The coupling surface was an air-filled parallelepiped of dimensions 0.9 × 0.6 × 2.65 m, centered in the contaminated air environment. The coupling surface employs the surface source write (SSW) functionality in MCNP 6.1.1, in which the photon distribution from the contaminated air source term at boundary of the coupling surface is recorded.

In the second step, the phantom was embedded in the center of the coupling surface and particles were transported from the coupling surface using the photon spectrum recorded in the previous step. This employs the surface source read (SSR) option in MCNP 6.1.1, in which the coupling surface obtained from the SSW acts as the photon source term. The organ dose rates were computed by scoring over the phantom. The SSW and SSR coupling surface is depicted in Figure 2 of Ref. [2]. All Monte Carlo calculations were performed on a small Beowulf computing cluster using several Intel Core i7 and Apple Mac Mini computers with Intel Core2Duo processors. Runtimes were in the order of 1×10^5 CTME (computational time as calculated by MCNP). Source particles were cut off after being under a minimal energy of 1×10^{-3} MeV.

Dose rate coefficients and derived quantities were calculated for eight monoenergetic photon energies at 30, 50, 100, 200, 500, 1000, 2000 and 5000 keV. The spectra recorded on the coupling surface for the emission of 100 keV, 1 MeV and 5 MeV photons are similarly used with the female phantom simulations, and depicted in Figure 3 of Ref. [2]. Organ dose rates were calculated in MCNP 6.1.1 using track-length fluence estimators to determine the energy-dependent fluence in the organs. The kerma approximation was employed by folding the fluence estimation with tissue-specific fluence-to-kerma coefficients as described in Ref. [14] and similarly employed in Ref. [2]. Simulations were run for the coupling surface in MCNP 6.1.1 until 10 million particles were transported in the coupling surface source calculation at 30 keV and until 100,000 particles were transported at 5 MeV. All particles were transported from the coupling surface source to the phantom. All organs required for the computation of effective dose identified in ICRP Publication 103[4] were considered. The organ dose error of the Monte Carlo calculation was typically under 5 % for the adrenals, one of the organs hardest to tally. Other organs doses had an even higher tally precision. With organ dose rate data from both male and female phantoms, the effective dose E was computed for the voxel and stylized phantoms using ICRP Publication 103 tissue weighting factors[4] as follows:

$$E = \sum_T w_T * H_T, \quad H_T = \sum_R w_R D_{T,R} \tag{1}$$

With organ T, the tissue weighting factor w_T, H_T equivalent dose H_T, radiation type R, radiation weighting factor w_R, absorbed dose $D_{T,R}$ in the volume of organ T due to radiation of type R.

RESULTS

Table 1 summarizes organ dose rate coefficients for three photon energies at 100, 1000 and 5000 keV. For each energy, the first and second columns show the dose rate coefficients for the voxel and the stylized female phantoms. The third column contains the ratio of the voxel divided by the stylized dose rate coefficient.

Figure 1 shows a plot of the organ dose rate coefficients for 100, 1000 and 5000 keV. The majority of the organs show slightly higher dose rate coefficients for the stylized phantom, having ratios between 0.8 and 1. Overall, the organ dose rate coefficients for the female ratios show greater variance than those for the male ratios. For the male phantoms, all dose rate coefficient ratios are in the range from 0.8 to 1.2. Notably for the female phantoms, the red marrow, the salivary glands, the small intestine and the uterus show organ dose rate coefficients significantly higher in the voxel than in the stylized phantom, with organ dose rate coefficients over 1.2.

Figure 2(a) shows the relative contribution of each organ to the effective dose for the voxel and the stylized phantom in the energy range from 10 to 5000 keV. Each effective dose value is normalized to 1. For visibility, the organs contributing to the remainder sum are shown in a separate plot (Figure 2(b)). For a given organ, the plot value is given as:

$$OrganContribution = \frac{w_T \cdot H_T}{E} \tag{2}$$

The ratio of the effective dose rates between voxel and stylized phantoms is shown in Figure 3. For energies above 100 keV the effective dose rate calculated with either type of phantom agree within 10%. The general trend shows an increase in effective dose rate in stylized phantoms with photon energy. Over ~500 keV, the effective dose rate is higher when estimated with the stylized phantom than with the voxel phantom.

DISCUSSION

A greater variance was observed between the voxel phantom and the stylized phantom for the female phantoms' organ dose rate coefficients than for the male phantoms, as noted above. This discrepancy can be explained by two main differences in the phantom setup: (1) geometry and dimension of the phantoms and (2) use of surrogate tissues in the stylized phantom.

The voxel phantoms for the male and the female are based on clinical tomography image sets of persons similar to the reference person having a height of 176 cm and a mass of 73 kg for the male and a height of 163 cm and a mass of 60 kg for the female[3]. The voxel phantoms also vary in width and depth, as well as in the size of the internal organs. The stylized phantom is a hermaphrodite (i.e., male and female organs housed in one phantom). The stylized phantom consequently has the same dimensions when regarded as a male or a female phantom. The height is 173 cm and the mass is 76 kg, which is comparable to the male voxel phantom but 6% larger in size and 21% higher in mass than the female voxel phantom. Table 2 compares basic properties of the male and female voxel phantom to the stylized phantom. Not only the mass of the stylized phantom itself but also the mass of the inner organs is more comparable to the male voxel phantom than to the female voxel phantom (see Table 8 in Ref. [4] for a comparison of the ICRP Publication 89[12] organ data, which serves as a basis for the ICRP Publication 110[3] voxel phantoms, to the organ masses used in the stylized phantom). Furthermore, the stylized phantom uses surrogate tissues for two organs, the extra-thoracic region and the lymph, for which the thymus acts as a surrogate.

As seen from Figure 1, the small intestine has the second largest difference between the voxel and the stylized phantom; the difference can be explained by the difference in organ masses, but more predominantly by organ volume and geometry (organ shape, distances), between the male and female phantoms. The small intestine has a 9% higher mass in the male voxel phantom than in the stylized, while it is 6% smaller in the female voxel phantom. The same discrepancy also explains the large difference in the organ dose coefficient rate for the red bone marrow. The thymus has a 2% higher mass in the male voxel phantom than in the stylized phantom, while it is 69% higher in the female voxel phantom than in the stylized phantom. Comparing the contribution of the organs to the effective dose (Figure 2) between the voxel and the stylized phantom shows that a large number of organs have comparable contributions in both phantoms and also comparable changes with increasing energy, while certain organs behave differently.

As depicted in Figure 2, the most dominant is the discrepancy in the relative contribution to the effective dose between the stylized and the voxel phantom is in the breast. While the contribution to the effective dose for the stylized phantom is 0.3, it is only 0.1 for the voxel phantom at 30 keV. The contribution of the breast in the voxel phantom increases slightly for higher energies but decreases in the stylized phantom with higher energies. At 5000 keV, the contribution in the stylized phantom has decreased to about 1.5, while the contribution in the voxel phantom has increased to about 0.2. For the lung and the red bone marrow, the contribution in the stylized phantom increases with higher energies, while the contribution in the voxel phantom stays relatively constant over the energy range.

Of the organs that ICRP considers as remainder (see Fig. 2(b)), the adrenals contribute roughly 2–3 times more to the effective dose in the stylized phantom than in the voxel phantom; other organs with higher contributions in the stylized phantom include thymus, spleen, and gall bladder. In contrast, the contribution of the small intestine to the effective dose is about twice as high in the voxel phantom. Overall, the contribution of the remainder organs to the overall effective dose is relatively constant at about 8% in the voxel phantom, while it increases with the energy from about 8% to 12% for the stylized phantom, over the energy range of 30 keV to 5000 keV. Again, this is due to variations in defined organ volume/geometry, organ proximity, and voxel resolution in defining the voxel and stylized phantoms.

CONCLUSIONS

Organ dose rate coefficients calculated for the adult female stylized and voxel phantoms were generally in good agreement between 30 and 5000 keV. Incorporating data from previous work with the adult male voxel and stylized phantom permitted calculation of effective dose as defined by ICRP Publication 103[10]; effective dose for the voxel and stylized phantoms differed within 8% at 100 keV and differed < 5% between 200 and 5000 keV. Differences in organ dose rate coefficients were attributed to organ position, shape, and phantom features. For example, the small intestine lining was modeled in the voxel phantom but was homogenized in the small intestine in the stylized phantom. However, the stylized phantom has sufficient resolution to model thin, sensitive walls,

which is not permitted by the resolution of the voxel phantoms. Overall, in the case of air submersion, organ doses between the voxel and stylized phantoms were well correlated, resulting in comparable values of effective dose.

ACKNOWLEDGEMENTS

The authors would like to thank Dr. Keith Eckerman and Dr. Michael Bellamy for their support.

This work was supported by the U.S. Environmental Protection Agency Office of Radiation and Indoor Air under Interagency Agreement number DOE 1886-T249-06/1886-T233-06 and was prepared by Oak Ridge National Laboratory, managed by UT Battelle, LLC, for the U.S. Department of Energy under contract DEAC05-00OR22725.

REFERENCES

1. Bellamy, M., Veinot, K., Hiller, M., Dewji, S., Eckerman, K., Easterly, C., Hertel, N. and Leggett, R. Effective Dose Rate Coefficients for Immersions in Radioactive Air and Water. Radiation protection dosimetry(2016).
2. Bellamy, M., Hiller, M., Dewji, S., Veinot, K., Leggett, R., Eckerman, K., Easterly, C. and Hertel, N. Comparison of Monoenergetic Photon Organ Dose Rate Coefficients for Stylized and Voxel Phantoms Submerged in Air. Radiation protection dosimetry, ncv548 (2016).
3. International Commission on Radiological Protection. *ICRP Publication 110: Adult Reference Computational Phantoms* **39** (2009).
4. Han, E. Y., Bolch, W. E. and Eckerman, K. F. Revisions to the ORNL Series of Adult and Pediatric Computational Phantoms for use with the MIRD Schema. Health Phys. **90**(2006).
5. Dillman, L. T. Absorbed Gamma Dose Rate for Immersion in a Semi-infinite Radioactive Cloud. Health Phys. **27**(1974).
6. Poston, J. W. and Snyder, W. S. A Model for Exposure to a Semi-infinite Cloud of a Photon Emitter. Health Phys. **26**(1974).
7. Kocher, D. C. Dose-Rate Conversion Factors for External Exposure to Photons and Electrons. Health Phys. **45**(1983).
8. Eckerman, K. F. and Ryman, J. C. *External Exposure to Radionuclides in Air, Water, and Soil, Federal Guidance Report No. 12* Publication EPA 402-R-93-081, Oak Ridge National Laboratory (1993).
9. Kramer, R., Khoury, H. J. and Vieira, J. W. Comparison between effective doses for voxel-based and stylized exposure models from photon and electron irradiation. Phys Med Biol. **50**(2005).
10. International Commission on Radiological Protection. *ICRP Publication 103: The 2007 Recommendations of the International Commission on Radiological Protection* **37** (2007).
11. Cristy, M. and Eckerman, K. F. *Specific Absorbed Fractions of Energy at Various Ages from Internal Photon Sources: Parts I-VII* Publication ORNL/TM 8381/V1-V7, Oak Ridge National Laboratory (1987).
12. International Commission on Radiological Protection. *ICRP Publication 89: Basic Anatomical and Physiological Data for Use in Radiological Protection: Reference Values* **32** (2002).
13. International Commission on Radiation Units and Measurements. *ICRU Report 46: Photon, Electron, Proton and Neutron Interaction Data for Body Tissues* (2002).
14. Pelowitz, D. B. *MCNP6 User's Manual Version 1.0* Publication LA-CP-13-00634, Los Alamos National Laboratory (2013).

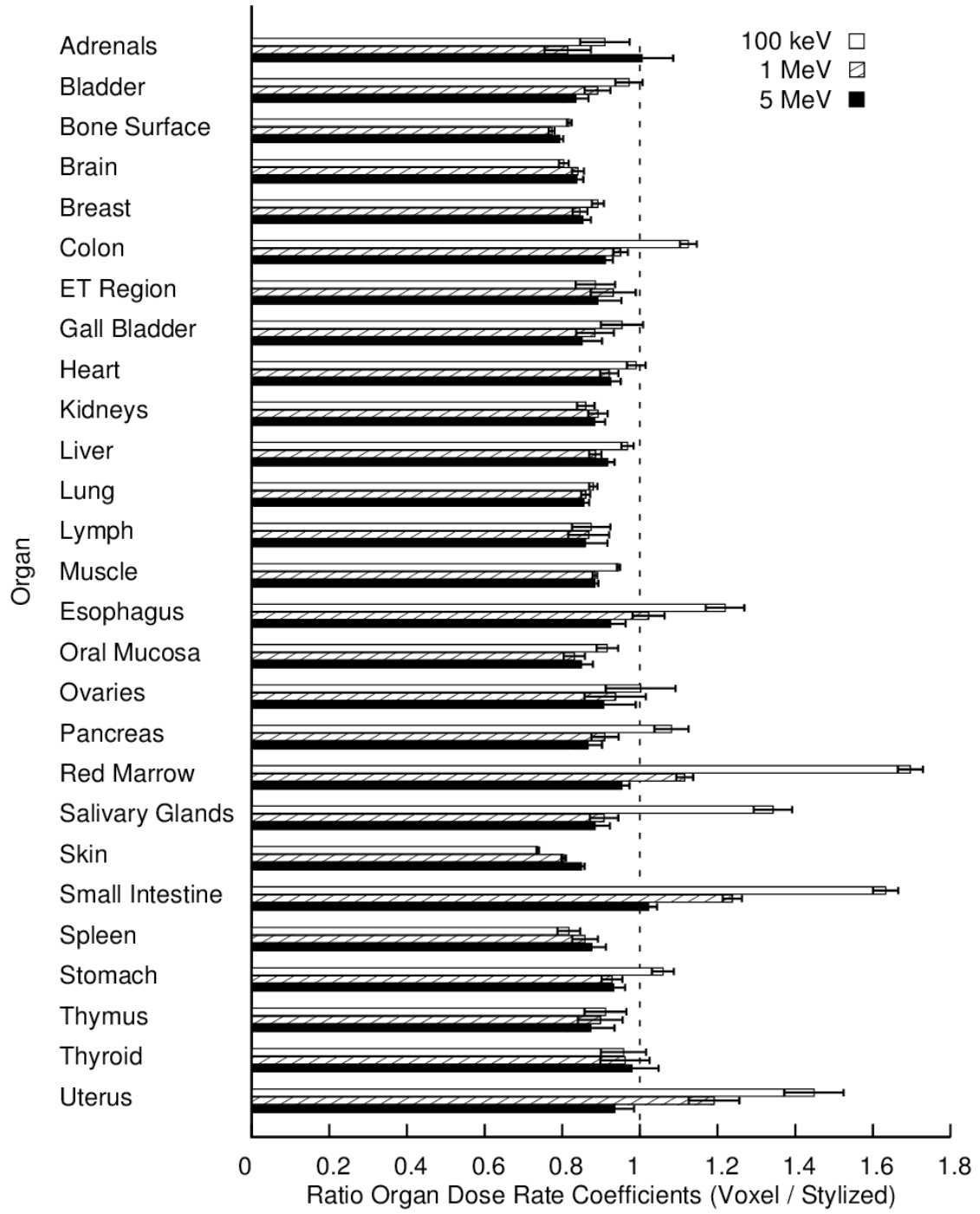

Figure 1: Ratio of organ dose rate coefficients for the female voxel / stylized phantom for 100 keV, 1 MeV and 5 MeV energies. The estimated tally precision of the Monte Carlo calculations was propagated into the given error of the ratio.

(a)

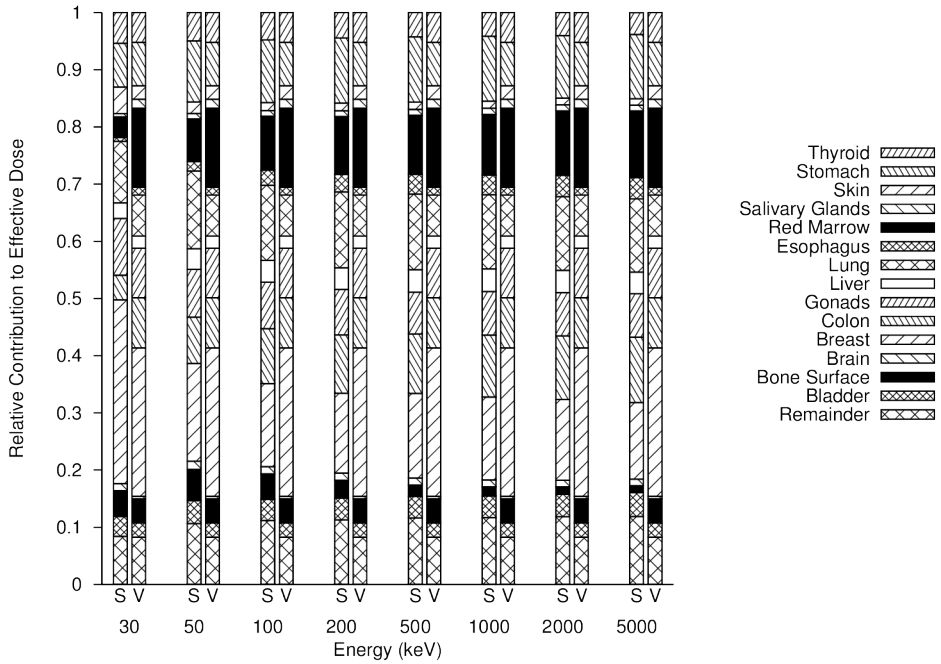

(b)

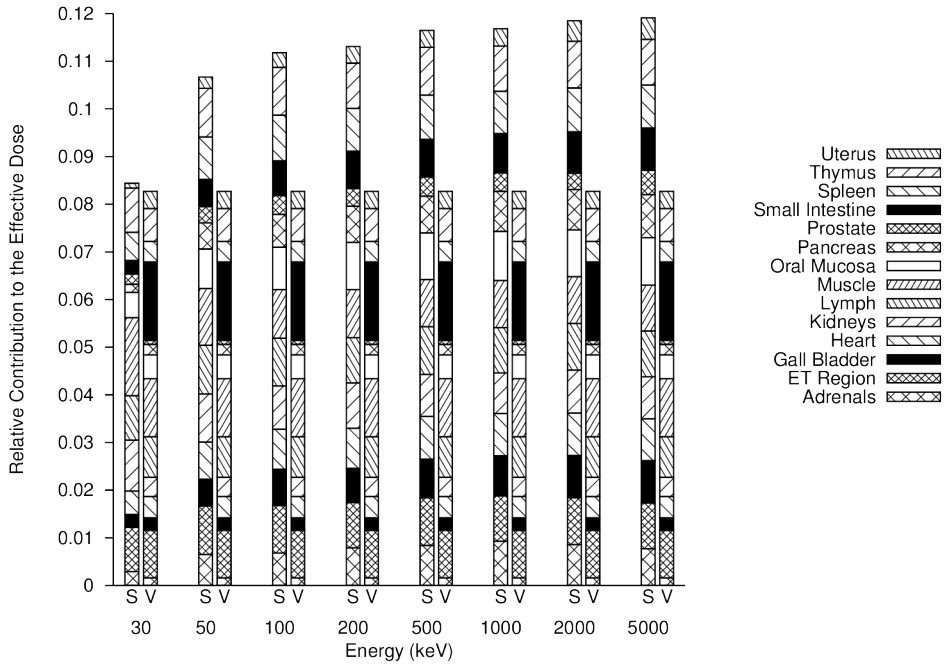

Figure 2: Contribution of the organs to the effective dose (a) based on the stylized (S) and voxel (V) computational phantoms (see marks below the columns). The organs comprising the remainder are shown in a separate plot (b). The order of the organs in each column matches the order in the legend.

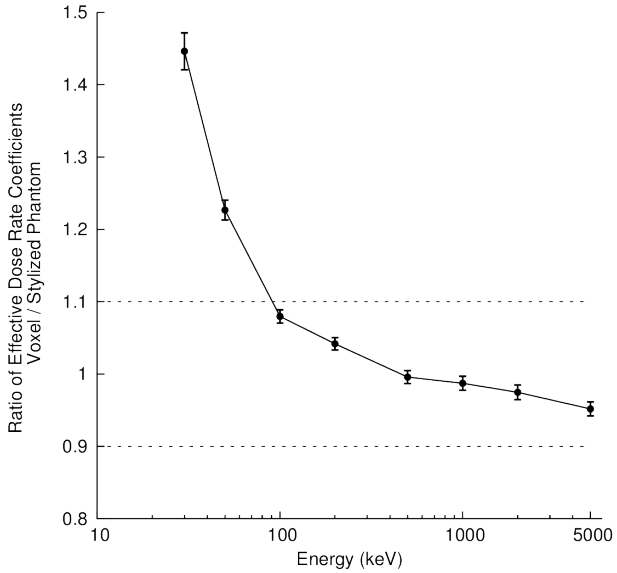

Figure 3: Ratio of effective dose rate coefficients between the voxel and the stylized adult phantoms.

Table 1: Organ dose rate coefficients for voxel and stylized phantoms (Sv m^3 Bq^{-1} s^{-1}), and voxel/stylized ratio.

	100 keV			1000 keV			5000 keV		
Organ	Voxel	Stylized	Ratio[a]	Voxel	Stylized	Ratio[a]	Voxel	Stylized	Ratio[a]
Adrenals	2.52E-15	2.77E-15	0.91(6)	3.68E-14	4.53E-14	0.81(6)	2.24E-13	2.23E-13	1.01(8)
Bladder	3.37E-15	3.46E-15	0.97(4)	3.79E-14	4.26E-14	0.89(3)	2.34E-13	2.80E-13	0.84(3)
Bone Surface	1.36E-14	1.66E-14	0.82(1)	5.43E-14	7.03E-14	0.77(1)	2.59E-13	3.26E-13	0.79(1)
Brain	3.81E-15	4.74E-15	0.80(1)	4.57E-14	5.44E-14	0.84(2)	2.59E-13	3.09E-13	0.84(2)
Breast	4.04E-15	4.53E-15	0.89(2)	4.58E-14	5.42E-14	0.85(2)	2.56E-13	3.00E-13	0.85(2)
Colon	3.38E-15	3.00E-15	1.12(2)	3.84E-14	4.04E-14	0.95(2)	2.33E-13	2.56E-13	0.91(2)
ET Region	3.58E-15	4.05E-15	0.89(5)	4.29E-14	4.61E-14	0.93(6)	2.49E-13	2.79E-13	0.89(6)
Gall Bladder	2.93E-15	3.07E-15	0.95(5)	3.61E-14	4.09E-14	0.88(5)	2.21E-13	2.59E-13	0.85(5)
Heart	3.39E-15	3.42E-15	0.99(2)	3.98E-14	4.33E-14	0.92(2)	2.36E-13	2.55E-13	0.92(3)
Kidneys	3.18E-15	3.70E-15	0.86(2)	3.70E-14	4.15E-14	0.89(3)	2.26E-13	2.56E-13	0.88(3)
Liver	3.46E-15	3.58E-15	0.97(2)	3.91E-14	4.42E-14	0.89(2)	2.33E-13	2.54E-13	0.92(2)
Lung	3.61E-15	4.10E-15	0.88(1)	4.16E-14	4.84E-14	0.86(1)	2.46E-13	2.87E-13	0.86(1)
Lymph	3.54E-15	4.05E-15	0.87(5)	4.00E-14	4.61E-14	0.87(5)	2.40E-13	2.79E-13	0.86(6)
Muscle	3.92E-15	4.14E-15	0.95(0)	4.25E-14	4.80E-14	0.88(1)	2.46E-13	2.78E-13	0.88(1)
Esophagus	2.99E-15	2.45E-15	1.22(5)	3.94E-14	3.85E-14	1.02(4)	2.33E-13	2.52E-13	0.92(4)
Oral Mucosa	3.31E-15	3.61E-15	0.92(3)	4.17E-14	5.02E-14	0.83(3)	2.46E-13	2.90E-13	0.85(3)
Ovaries	2.77E-15	2.77E-15	1.00(9)	3.45E-14	3.69E-14	0.94(8)	2.21E-13	2.44E-13	0.91(8)
Pancreas	3.01E-15	2.79E-15	1.08(4)	3.72E-14	4.09E-14	0.91(4)	2.27E-13	2.62E-13	0.87(4)
Red Marrow	5.00E-15	2.95E-15	1.70(3)	4.41E-14	3.96E-14	1.12(2)	2.48E-13	2.60E-13	0.95(2)
Salivary Glands	5.00E-15	3.72E-15	1.34(5)	4.41E-14	4.86E-14	0.91(4)	2.48E-13	2.80E-13	0.88(4)
Skin	3.87E-15	5.26E-15	0.74(0)	4.47E-14	5.57E-14	0.80(1)	2.55E-13	3.01E-13	0.85(1)
Small Intestine	4.81E-15	2.95E-15	1.63(3)	4.90E-14	3.96E-14	1.24(2)	2.66E-13	2.60E-13	1.02(2)
Spleen	3.20E-15	3.91E-15	0.82(3)	3.69E-14	4.30E-14	0.86(3)	2.29E-13	2.61E-13	0.88(4)
Stomach	3.62E-15	3.42E-15	1.06(3)	3.93E-14	4.24E-14	0.93(3)	2.34E-13	2.51E-13	0.93(3)
Thymus	3.69E-15	4.05E-15	0.91(5)	4.14E-14	4.61E-14	0.90(6)	2.44E-13	2.79E-13	0.87(6)
Thyroid	4.29E-15	4.48E-15	0.96(6)	4.45E-14	4.63E-14	0.96(6)	2.50E-13	2.55E-13	0.98(7)
Uterus	3.69E-15	2.55E-15	1.45(8)	4.14E-14	3.47E-14	1.19(7)	2.44E-13	2.61E-13	0.94(5)
Effective Dose	4.04E-15	3.74E-15	1.08(1)	4.42E-14	4.48E-14	0.99(1)	2.56E-13	2.69E-13	0.95(1)

[a] Uncertainty of the last significant digit in parentheses, for example 0.91(6), refers to the quantity, 0.91 ± 0.06.

Table 2: Comparison of male and female voxel phantom and stylized phantoms, see Table 8 in (4). Compared are sizes and masses of the phantoms as well as organs

	Voxel Male	Voxel Female	Stylized
Height (cm)	176	163	173
Mass (kg)	73.0	60.0	75.3

Organs mass differences (%)	Male Voxel Phantom to Stylized	Female Voxel Phantom to Stylized
> 20	Larynx, Trachea	Larynx, Thymus, Thyroid, Trachea
15 ≤ x < 20	Esophagus	Adrenals, Colon (wall and contents), Lungs (with blood), Stomach (wall and contents)
10 ≤ x < 15	Colon (contents), Pancreas, Testes	Colon (contents), Pancreas, Urinary bladder (wall), Breast
5 ≤ x < 10	Brain, Eyes, Heart (contents), Liver, Prostate, Skeletal regions, Small intestine (wall and contents), Urinary bladder (wall),	Brain, Esophagus wall, Kidneys, Small intestine (wall and contents), Rest of body
< 5	Adrenals, Colon (wall), Gall bladder (wall and contents), Heart (wall), Kidneys, Lungs, Rest of body, Salivary glands, Skin, Spleen, Stomach (wall and contents), Thymus, Thyroid	Gall bladder (wall and contents), Heart (wall and contents), Liver, Ovaries, Salivary glands, Skeletal regions, Skin, Spleen, Uterus